2022

PRELIMINARY STUDIES OF BACKGROUND REJECTION CAPABILITIES FOR THE SOUTHERN WIDE–FIELD GAMMA–RAY OBSERVATORY

Sonali Mohan
Michigan Technological University, sonalim@mtu.edu

PRELIMINARY STUDIES OF BACKGROUND REJECTION CAPABILITIES FOR THE SOUTHERN WIDE−FIELD GAMMA−RAY OBSERVATORY

By

Sonali Mohan

A REPORT

Submitted in partial fulfillment of the requirements for the degree of

MASTER OF SCIENCE

In Physics

MICHIGAN TECHNOLOGICAL UNIVERSITY

2022

This report has been approved in partial fulfillment of the requirements for the degree of MASTER OF SCIENCE in Physics.

Department of Physics

Report Advisor: *Dr. Petra H. Huentemeyer*

Committee Member: *Dr. David Nitz*

Committee Member: *Dr. Brian Fick*

Committee Member: *Dr. Ravindra Pandey*

Department Chair: *Dr. Ravindra Pandey*

Dedication

To my Family, teachers and friends

who didn't hesitate to criticize my work at every stage - without which I would neither be who I am nor would this work be what it is today.

Contents

List of Figures

List of Tables

Acknowledgments

I wish to express my deep sense of gratitude to my advisor Prof. Dr. Petra H. Huentemeyer, for having permitted me to carry out this project work.

I would also like to thank my colleague, Dr. Xiaojie Wang. Without her guidance and persistent help this work would not be possible.

I would also like to mention Prof. Dr. Andrew J Smith, Chad Brisbois and Dezhi Huang for providing me the SWGO related resources and continuous feedback on my work.

I would also like to acknowledge the support of the Department of Physics at Michigan Technological University for providing technical resources and the support throughout my study.

Finally, yet importantly, I would like to express my heartfelt thanks to my beloved Family and Friends and Gurudev for their blessings, support and wishes for the successful completion of this project.

Sonali Mohan

List of Abbreviations

COM	centre of mass
CTA	Cherenkov Telescope Array
CORSIKA	COsmic Ray SImulations for KAscade
EAS	Extensive Air Shower
Fermi-LAT	Large Area Telescope
WCD	water Cherenkov detector
NKG	Nishimura-Kamata-Greise
HAWC	High-Altitude Water Cherenkov
H.E.S.S.	High Energy Stereoscopic System
IACT	Imaging Atmospheric Cherenkov Telescope
LHAASO	Large High Altitude Air Shower Observatory
LDF	Lateral Distribution Function
LC	lower cell
MAGIC	Major Atmospheric Gamma Imaging Cherenkov
PE	photoelectron
PMT	photomultiplier tube
RMS	Root Mean Square
SWGO	Southern Wide-field Gamma-ray Observatory

UC	upper cell
VERITAS	Very Energetic Radiation Imaging Telescope Array System

Abstract

The Southern Wide-field Gamma-ray Observatory (SWGO), is a next-generation gamma-ray observatory to be constructed in the Southern Hemisphere that will complement current and future instruments by providing a wide-field coverage of a large portion of the southern sky and a better sensitivity to the 100 GeVs to few PeVs photon band to understand extreme astrophysical phenomena throughout the universe. Air shower events initiated by gamma rays will be recorded by the detector and reconstructed to extract shower properties. The challenge for air-shower arrays in the observation of gamma-ray sources is the large background of hadronic cosmic rays. Thus, the identification and separation of this background is critical. In this report, I present a performance study of gamma-hadron separation parameters for the SWGO observatory using simulation data a study with a specific parameters that measures the smoothness of the footprint in the detector array was conducted and results achieved with a SWGO reference configuration were compared to results confirmed with the High-Altitude Water Cherenkov(HAWC) Observatory.

Chapter 1

Introduction

From the beginning of time, some of our most intriguing questions have been regarding the nature of the universe, the heavenly bodies that surround us, or are farther away from us. In the last two centuries, innovations in physics, electronics, and eventually computers have allowed the field of Astronomy to answer some of these questions, but the unanswered ones are as vast as space itself.

Today, thousands of telescopes operate in space and earth-bound across the globe, with astronomers capturing new perspectives of the universe—and new knowledge every day. Our comprehension of the universe is derived from observations of radiation over an enormous range of energies we detect from different sources in the universe utilizing these telescopes. These telescopes observe either thermal or non-thermal

radiations.

The bulk of photons propagating within the universe and detected on the Earth are thermal radiation. The thermal radiation is produced by processes including the Cosmic Microwave Background (CMB), thermal emissions from the stars, or the accretion disks around neutron stars and other massive objects and follows a black-body spectrum. Black-body radiation is a type of electromagnetic radiation that a black body, which absorbs all electromagnetic radiation, emits to stay in thermal equilibrium. The spectrum of black-body radiation only depends on the temperature of the source. Thermal radiation can reach the kilo electron volt (keV) energy range and beyond(to MeV). However, there are other photons, for example, the cosmic gamma rays, from 1 TeV to several PeV, which are well beyond the energy range reached by thermal emission. These photons are produced by non-thermal collective mechanisms, meaning that their emission results are not from black-body radiation yet instead from fundamental interactions among the particles themselves. The study of this radiation interests astrophysicists because it involves physical processes that are impossible to emulate in our earth-bound laboratories at these high energies. The photons or particles produced by non-thermal processes follow a power-law spectrum, instead of a black body spectrum, which is given by [7]

$$\frac{dN}{dE}\alpha E^{-\Gamma} \tag{1.1}$$

where, Γ is the spectral index, E is the energy and $\frac{dN}{dE}$ is the differential energy spectrum.

Moreover, observing the non-thermal universe is strenuous. One apparent reason for this is the dominance of the radiation from thermal processes. Thus, x-ray and gamma-ray observational techniques are widely applied to study the non-thermal phenomena[8].

1.1 Gamma-Ray Astronomy

Gamma rays are photons with the highest energies in the electromagnetic spectrum that range from 100 kilo electron Volts(keV) to a few 100 Terra electron Volts(TeV). Traditionally, based on the energy per photon, gamma rays are outlined as low (MeV), high (GeV), very high (TeV), ultra-high (PeV). They, therefore, provide information about the most energetic processes and phenomena within the universe. Gamma rays being neutrally charged particles will not be deflected in the interstellar magnetic fields and will point back to their sources of origin[9].

The GeV-TeV gamma rays are essential in the study of both galactic as well as extragalactic astronomy. The study of sources of very high energy cosmic radiation,

for example, include black holes, neutron stars, active galactic nuclei, supernovae, kilonova, supernova remnants, and gamma-ray bursts. It also involves astrophysical phenomena like propagation and acceleration of the very high energy cosmic rays in which conventional physics operates under extreme conditions. The Galactic gamma-ray emission includes the emissions from pulsars, pulsar wind nebulae, supernova remnants, compact object binaries, and the Galactic diffuse emission. The discrete gamma-ray sources produce gamma rays near the acceleration sites of cosmic rays. The diffuse emission is produced when the cosmic rays interacts with the interstellar medium.

The study of Very High Energy(VHE) gamma rays is one of the enlightening yet challenging frontiers in Astrophysics. The hard work by several scientists over the decades revealed that several processes occurring in the Universe would result in gamma-ray emission. These processes include interactions of cosmic rays with interstellar gas, and interactions of energetic electrons with magnetic fields. Since the development of the first technique for their detection in the 1960s, scientists have been searching and studying these emissions. The first detection of significant gamma-ray emission from our galaxy was made in 1967 by the gamma-ray detector aboard the OSO-3 satellite, and it detected 621 gamma rays, including the first gamma-rays from outside our galaxy [10]. Since then, data from the satellites confirmed the existence of gamma-ray background, also produced the first detailed map of the sky at gamma-ray wavelengths, and detected a plethora of sources.

1.2 Gamma ray production processes

There are two main classes of gamma-ray production: leptonic, where the gamma rays emitted from interactions of electrons, and hadronic, where the gamma rays are released from particle decay.

1.2.1 Leptonic production

There are two leptonic processes that are described here.

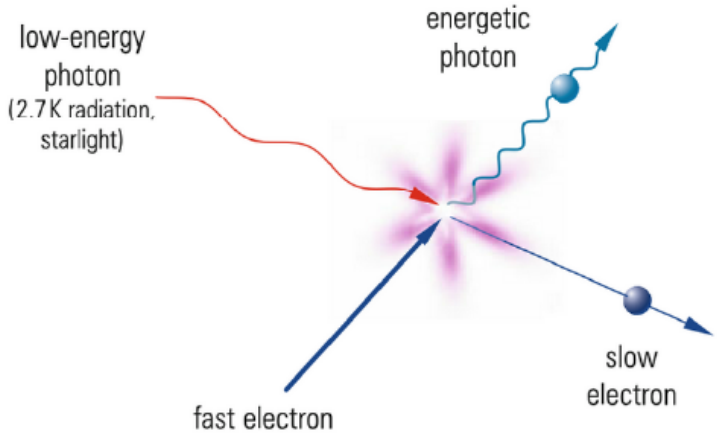

Figure 1.1: Inverse Compton scattering of a low energy photon[1].

1.2.1.1 Inverse Compton Scattering

The electron population that can scatter off of ambient photons in the vicinity of the source for example, in CMB, star light, or IR from dust. The photons receive some of the electron's energy during this process, boosting their energy. This leptonic process is known as "inverse Compton scattering". The ambient photons may be the synchrotron photon, are sometimes referred to as "synchrotron self-Compton"[8]. This leads to a spectral energy distribution that has two peaks: one at lower energies (1 keV) for the synchrotron component, and another in the GeV-TeV range for the inverse Compton component. The position of the peak is determined by a wide variety of factors, such as the magnetic field[8].

1.2.1.2 Bremsstrahlung Process

A third type of leptonic emission, bremsstrahlung, primarily occurs at lower energies. German for "braking radiation", bremsstrahlung occurs when a charged particle is deflected by another charged particle, resulting in the emission of a photon.

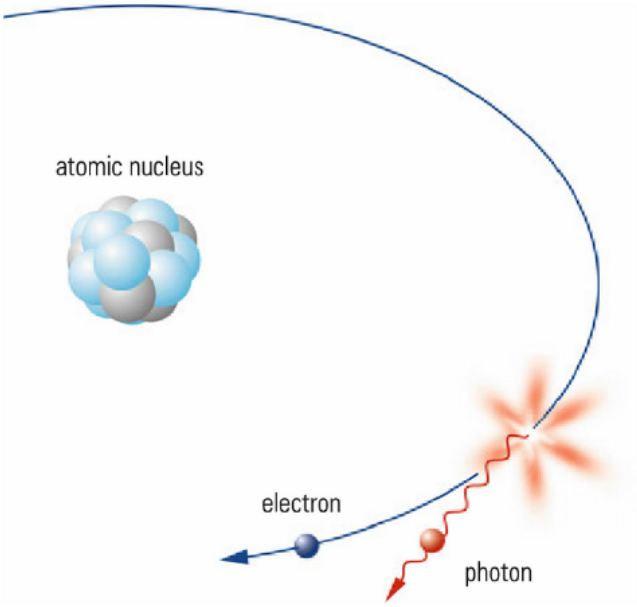

Figure 1.2: Bremsstrahlung emmision [1]

1.2.2 Hadronic Production

The decay of neutral pions(π_0) that are produced by the interaction of cosmic rays with interstellar medium (ISM) causes emission of gamma rays[7].

1.3 Gamma-Ray Observation

Earth's atmosphere is opaque to gamma rays, especially lower energies gamma rays, which makes direct detection on the ground impossible. Thus it is sensible to launch detectors above the atmosphere, and, space-based instruments on-board balloons or

satellites are preferred. However, space-based telescopes have their own limitations owing to their insufficient detection area for the detection of VHE and UHE gamma rays. In such a situation, a ground-based detector is a better solution. Cosmic gamma-ray detectors are broadly classified as: space-based, and ground-based, each of which uses different detection techniques.

1.3.1 Space-based detectors

Space-based gamma-ray instruments are located beyond Earth, either in orbit around the planet or in deep space allowing direct observation of the gamma-ray photons and employ the principle of pair-creation by the incident gamma-ray in the detector to detect the gamma-ray signals [7]. The most prominent space-based gamma-ray detector is Fermi-LAT(Large Area Telescope) Gamma-ray Space Telescope. Fermi is capable of detecting gamma-ray emission from 20 MeV to beyond 1 TeV range[11].

1.3.2 Ground based detectors

The very-high-energy gamma-ray sky can be surveyed on a daily basis by particle-detector arrays at high (mountain) elevation. The limitations of launching larger spacecraft, instruments that are capable of detecting TeV gamma rays preferred to

be constructed on the ground. As the Earth's atmosphere blocks most of the gamma rays, these ground-based instruments employ the Earth's atmosphere as an intrinsic part of the detection technique. Thus, understanding the interaction of gamma rays with the molecules in the atmosphere is essential.

Ground-based observatories can probe a higher energy range than space-based observatories, as their effective areas can be many orders of magnitude larger than a space based telescope. Some of the ground-based gamma-ray observatories include HAWC(High-Altitude Water Cherenkov Observatory), MAGIC(Major Atmospheric Gamma Imaging Cherenkov), H.E.S.S.(High Energy Stereoscopic System), VERITAS(Very Energetic Radiation Imaging Telescope Array System), LHAASO(Large High Altitude Air Shower Observatory) and upcoming SWGO(Southern Wide-field Gamma-ray Observatory). These are discussed in subsequent sections.

1.4 Ground based Gamma-Ray Astronomy

The ground-based gamma-ray astronomy is based on studying Extensive air showers (EAS). Extensive air showers were discovered by Rossi, Schmeiser, Bothe, Kolhorster, and Auger at the end of the 1930s. The fundamental contributions of Bothe and Rossi, and by a cosmic-ray group at Massachusetts Institute of Technology, USA laid the foundation for many of the methods and much of the instrumentation used today in

the field of gamma-ray astronomy. Several works by the Japanese and US groups in the early 1970s led to many important experimental breakthroughs in VHE gamma-ray astronomy [12].

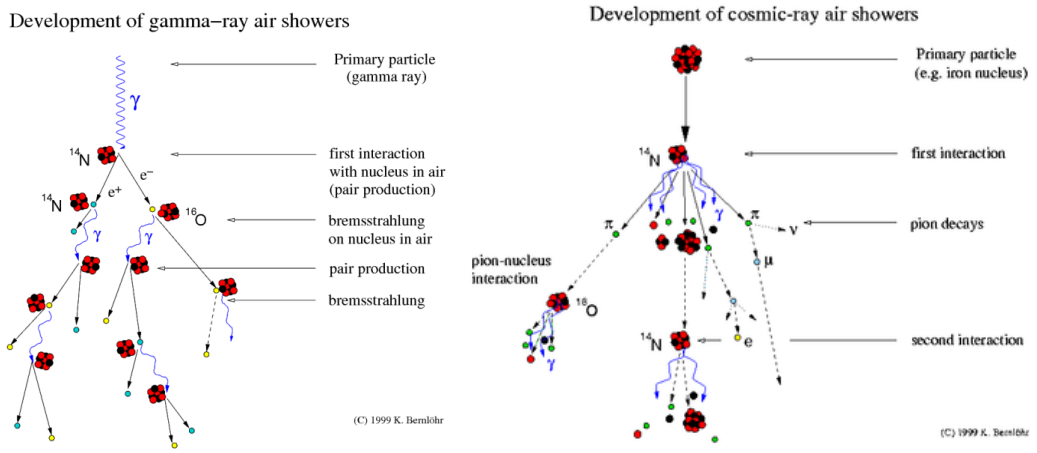

Figure 1.3: Extensive Air Shower production in the atmosphere [2]

1.4.1 Air Shower

An air showers are cascade of ionized particles and electromagnetic radiation produced in the atmosphere when a primary gamma/cosmic ray from space enters the atmosphere. There are categories of shower based on their primary source of production: Gamma-ray(electromagnetic) showers and cosmic-ray(hadronic) showers, as shown in figure 1.3

As a high-energy gamma-ray photon enters the atmosphere, it collides with a nucleus, producing an electron-positron pair. The secondary electron and positron

share the energy of the primary gamma ray and produce secondary gamma rays by the bremsstrahlung process, which is an initiator of further pair production.

Approximately, in each radiation length, a particle produces two more secondary particles that share the energy of the primary gamma ray. This iterative process creates a cascade of secondary particles, which constitutes the extensive air shower (EAS)[7].

As the penetration depth of the EAS increases, the number of secondary particles increases. The cascading process drops off after the average energy of the secondary electrons and positrons drops to 80 MeV, which is the critical energy at which the cross-section for ionization losses becomes comparable to that for Bremsstrahlung. This is known as shower maximum. Beyond this point, the number of secondary particles in the air shower plummets thus, the ionization losses halt the production of further air shower particles[11].

In a gamma-ray air shower, the secondary particles are ultra relativistic and the dominating processes sharply peak forward. Consequently, the air shower particles form a thin front, of only a few meters thick, referred to as the shower front which spreads laterally, to the order of one hundred meters owing to Coulomb scattering. The shape of the shower front is often described as a pancake[13].

In a hadronic air shower, high energetic cosmic particles collide with a nucleus in

the atmosphere, new particles are created. These new particles propagate in the same direction as the primary particle, and collide again to create new particles. This leads to a cascade of secondary particles that are moving at near light speed. As long as the energy of the particles is high enough to make new ones, the shower continues to grow by inelastic collisions. A large number of muons are produced in this process that travel far from the shower core and produce higher measured charge, and the presence of high energy muons indicate that it is more likely to be a hadronic shower.

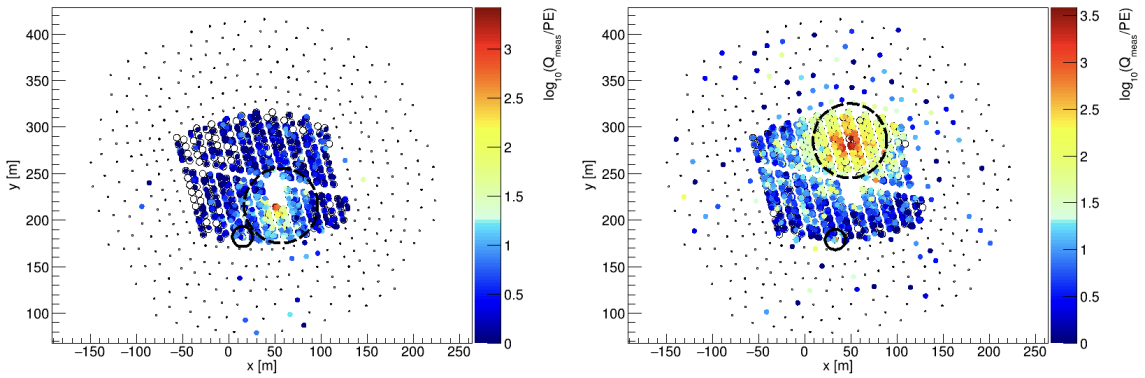

Figure 1.4: Extensive Air Shower footprints on the HAWC detector array. The figure on the left shows a gamma-ray shower and one the right a hadronic shower. The dashed-black circle marks the radius of 45 m from the shower core and the smaller black solid circle denotes the location of maximum charge outside that radius. [3]

Ground-based gamma-ray instruments observe the EAS particles and reconstruct the primary gamma rays based on the observable parameters from the secondary particles. The footprints of both kinds of shower are shown the figure 1.4

1.4.2 Air Shower Detection Techniques

There are two principle techniques of measuring EAS produced by the primary gamma rays.

1. Imaging Atmospheric Cherenkov Telescopes (IACTs),

2. Air Shower Particle Detectors (ASPDs).

Both types of detectors have complementary capabilities and hence, together they provide a more complete view of the sky at very high energies. ASPDs are surpassing IACTs in sensitivity at about 10 TeV (assuming 50 hours of observation time for IACTs and 1 year for ASPDs).The differences between both types are summarized in the Table 1.1.

Characteristics	IACT	ASPD
Field of View	3°-10°	90°
Duty Cycle	10-30%	$> 99\%$
Energy Range	50 GeV - $>$ 100 TeV	500 GeV - $>$ 100 TeV
Angular Resolution	0.05°-0.2°	0.1°-0.4°
Energy Resolution	$\sim 7\%$	20-60%
Background Rejection	$> 95\%$	90-99%

Table 1.1
Performance of IACT versus ASPD, adapted from [6]. For the IACT performance, it was assumed that a point-like source is observed for 50 hours/year.

1.4.3 Cherenkov Radiation

A process which some of the gamma-rays detection techniques utilize is cherenkov radiation. Cherenkov radiation is emitted when a charged particle travels at a speed greater than the phase velocity of light in that medium, in the shape of a cone of optical to UV light around the direction of the particle. This effect was first observed by Pavel Cherenkov in 1934 [13]. The half angle of the cone θ, called the Cherenkov angle can be derived as a ratio of the phase velocity of the light(c) and the refractive index(n):

$$\cos\theta = \frac{\frac{c}{n}}{v_{particle}} \tag{1.2}$$

where, $v_{particle}$ is the velocity of particle in that medium. The cherenkov angle is an important parameter used for the design consideration of ground-based detectors.

An IACT detects the Cherenkov radiation of the EAS in the atmosphere directly whereas ASPD Water Cherenkov detectors detect the Cherenkov light produced by EAS particles reaching water filled detectors on the ground.

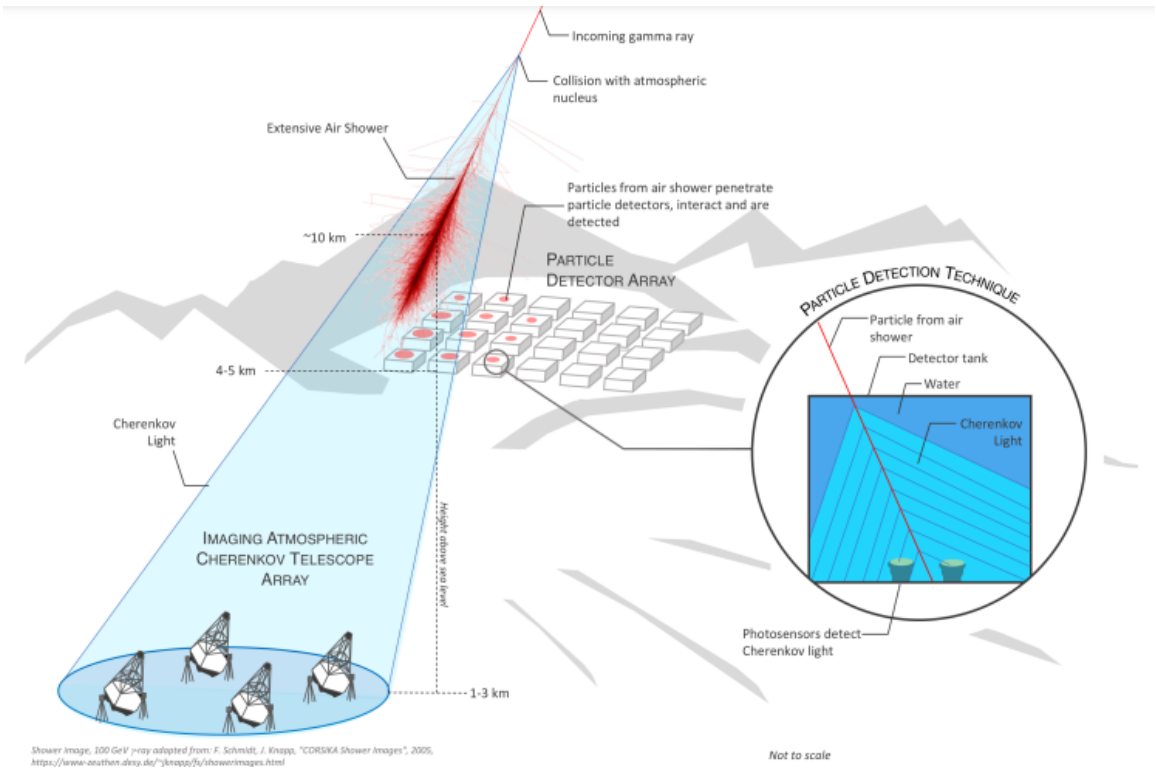

Figure 1.5: Ground based detectors: IACT and WCD [4]

1.4.4 Imaging Air Cherenkov Telescopes

IACTs detect the EAS as they develop in the atmosphere by detecting the Cherenkov light emitted by the charged particles in the EAS. The prominent IACT arrays are: MAGIC, H.E.S.S., VERITAS and CTA, which is under construction, more details can be found in [14],[15],[16],[17].

1.4.5 Air Shower Particle Detectors

An alternate way to detect EAS is to detect secondary charged particles in the shower that reach the ground where arrays of particle detectors are stationed. They have a higher energy threshold and larger angular resolution compared to IACTs. Due to their large field of view of the order of 2 steradians and high $> 95\%$ duty cycle, they are capable of performing unbiased sky surveys and are better suited for extended source ($> 1^{\circ}$) analyses. There are different types of ASPDs distinguished by the technologies they used to detect EAS particles: scintillation counters, resistive plate chambers, and water cherenkov detectors (WCDs). In a water Cherenkov detector, the water is dense (relative to air), and so photons, that are abundant in EAS in this altitude, produce e^+e^- (electron/positron) pairs once they enter the water. The Cherenkov radiation is emitted as these charged particles speed through the water. This Cherenkov radiation is detected by photomultiplier tubes (PMTs) installed inside the WCDs. In the report I will focus on WCDs. Below three examples of WCD-based observatories are given.

1.4.5.1 HAWC

High Altitude Water Cherenkov Observatory (HAWC) is a gamma-ray and cosmic ray observatory located at an altitude of 4100 meters, on the flanks of the Sierra

Negra volcano in the Mexican state of Puebla. HAWC is an EAS array of WCDs.

The WCDs in HAWC are corrugated steel tanks 5 meters high and 7.3 meters in diameter. Each tank contains a watertight bladder and four photomultiplier tubes (PMTs) which are sensitive at UV wavelengths. Three of the four photomultipliers are 8-inch hemispherical Hamamatsu PMTs and are placed on the bottom of the tank facing upward, and spaced 1.8 meters from the center of the tank. The fourth, a 10-inch Hamamatsu PMT, positioned at the bottom of the tank in the center, is a high quantum-efficiency PMT designed to improve the sensitivity of the observatory to low-energy showers. HAWC is capable of detecting primary cosmic rays with energies between 100 GeV and 100 TeV[18].

1.4.5.2 LHAASO

The Large High Altitude Air Shower Observatory (LHAASO) is a gamma-ray and cosmic-ray observatory located in Daocheng, Sichuan, China. The observatory is at an altitude of 4,410 metres above sea level. The observatory covers an area of some 145 hectare and has three underground observing pools containing 18 telescopes for capturing high-energy photons[19]. The observatory has been operational since April 2019.

1.4.5.3 SWGO

The SWGO is a gamma-ray observatory to be constructed in South America. SWGO will be the first high-altitude gamma-ray observatory to provide wide-field coverage of a large portion of the southern sky. It will complement current and future instruments, such as HAWC, LHAASO, and CTA.

SWGO will join the worldwide multi-messenger effort to unveil extreme astrophysical phenomena. Based primarily on water Cherenkov detector units, will cover an energy range from 100s of GeV to several PeV[20]. More details about the SWGO will be given in the following chapter.

Chapter 2

Southern Wide-Field Gamma-Ray Observatory

The SWGO collaboration is the recently established international organisation that intends to develop a detailed plan for a next-generation facility in the southern hemisphere. To date no such facility has ever been operated in the southern hemisphere, leaving a key part of the gamma-ray sky unobserved. 52 research institutions from twelve countries have signed the agreement for the international research and development collaboration.

The SWGO collaboration will conduct site selection and detector optimization studies prior to construction, with full operations foreseen to begin in 2026.[21] In this

chapter, SWGO is discussed briefly.

2.1 Introduction to SWGO

The SWGO is a project for a new generation of extensive air shower detectors, based primarily on the water Cherenkov technique, operating in the TeV gamma-ray energy range. It will supplement the capabilities of CTA which is an array of more than 100 IACTs, working as a multi-messenger instrument for the monitoring of transient and variable phenomena. It will expand the sky coverage of Northern Hemisphere facilities like HAWC and LHAASO, thus granting access to the entire Galactic Plane and most importantly, the Galactic Center.[22]

SWGO aims to achieve excellent sensitivity over a very large target energy range from about 100 GeV to the PeV, and improve on the performance of current sampling array instruments in all observational parameters, including energy and angular resolution, background rejection, and single-muon detection capabilities. The detector is planned to be deployed at a high-elevation site in the South American Andes hence, some sites in Chile, Argentina, Peru and Bolivia are under consideration.

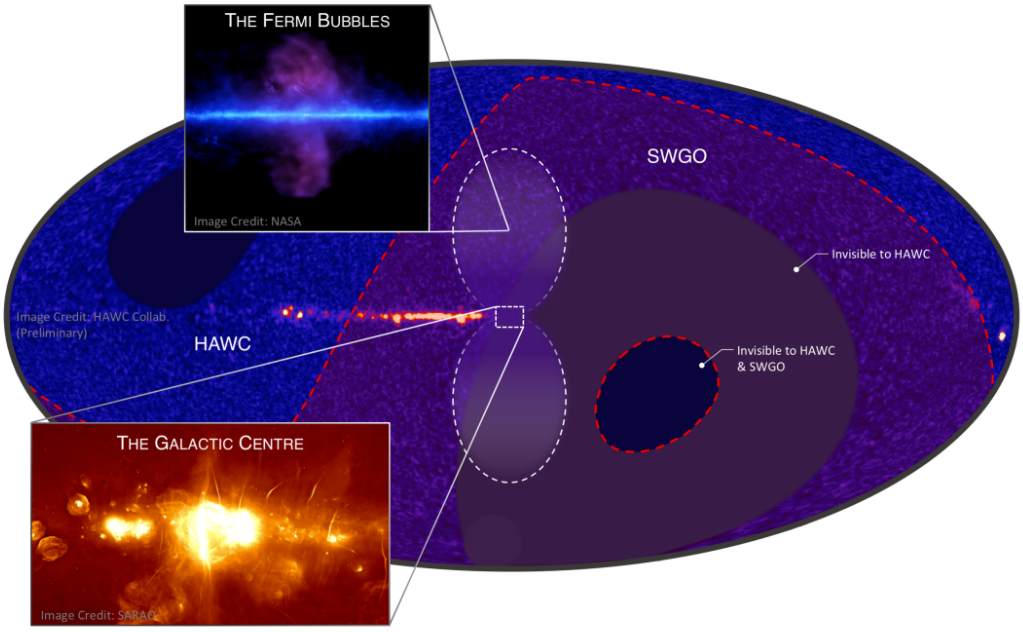

Figure 2.1: SWGO field of view [4].

2.2 Site Selection

The very-high-energy gamma-ray sky can be surveyed on a daily basis by particle-detector arrays at high elevation. The altitude at which the EAS has its maximum depends on energy. SWGO aims for being installed at a minimum altitude of 4.4 km a.s.l. in order to reach a low energy range, of few hundreds of GeV, besides detecting gamma-rays with energies up to several hundreds of TeV. Also, the larger the array, the higher the energy reach of the instrument. The reference configuration design for SWGO comprises an array of about 5,000 WCD tanks stationed over a circle of 300 m diameter, about 80,000 m^2 area.[23] The area of the single unit/cell is about 10

m^2. Thus, for the reference configuration, this translates into a minimum required instrumented area of about 80,000 m^2 and a minimum of 2.8×10^5 m^3 of purified water.

The site chosen must be a flat plateau of at least 300 m diameter, possibly up to 1000 m diameter, and it will host thousands of detector units, to be operated with minimum maintenance over the year. The detector characteristics must be taken into account when choosing the site for the installation of SWGO. [24]

Water scarcity might be a challenge in some sites. Environmental factors must be considered along with the interest of the local communities and stakeholders must be respected.

The SWGO consortium has issued a call for candidate sites in 2019 that will end with a short list of selected sites toward the June 2022. Preliminary site searches have found several candidate sites in the South American Andes mountain range in Argentina, Bolivia, Chile and Peru. [22]

2.3 Design Considerations

The SWGO Collaboration is in the process of designing and prototyping a wide field of view, high-duty-cycle ASPD array for SWGO which will complement CTA,

HAWC and LHAASO for the observation of transient and variable multi-wavelength and multi-messenger phenomena. For a gamma ray of given direction and energy, the charge signals from EAS particles recorded by the detector array provide the information available for reconstruction. The distribution of signals in the detector array is used in algorithms that are used to distinguish gamma-ray initiated showers from hadron initiated showers and is affected by observatory configurations.

2.4 Detector Designs and Configurations

Three configuration choices for the detector concept and its components are still under consideration. Three approaches are being considered for the construction of the core detector array:

- Cylindrical corrugated steel tanks or alternatively Rotoplas tanks
- Artificial ponds
- Bladders floating in a natural lake

The three approached provide different trade-offs in terms of required costs, labour, materials for constructions. The descriptions of three approaches are given in reference [6]. In the following the design used for the study presented in this report will be discussed in more detail.

2.5 Considered Design

The SWGO detector unit is proposed to be a double-layer water Cherenkov detector. Detector array will be constructed from these optically isolated units densely packed together. The upper cell has a large photomultiplier-tube (PMT) of 8" diameter installed at the cell floor facing upward, to measure the arrival time of direct Cherenkov light, which is essential for accurate timing to be used for direction reconstruction. The bottom compartment has a downward facing 8" diameter PMT to perform muon identification.

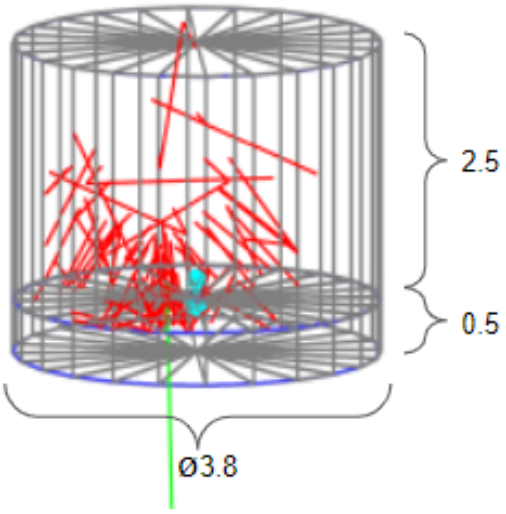

Figure 2.2: SWGO WCD unit. [5]

The upper layer is 2.5m deep and the lower layer is 0.5m deep. The bottom chamber of the detection unit serves a dual purpose: muon identification and enhancing the

dynamic range. At the energies of the order of GeV, muons travel straight through and deposit a significant amount of Cherenkov light in both top and bottom chambers. Gamma rays and electrons will cascade in the top chamber and only a small fraction of this cascade reach the bottom chamber. Hence, the light ratio between the top and bottom chamber is helpful in identifying muons. Furthermore, the bottom chamber provides a large dynamic range in the shower core, for the highest energy gamma rays with the high particle density. Even though, the PMTs in the upper cell will saturate, only a few particles will penetrate to the lower cell which can provide a good estimate of the particle density to aid the high-energy performance of the observatory.

The walls of the units are lined with white diffusive reflective material, like Tyvek, very similar to Pierre Auger Observatory, significantly enhancing the number of detectable particles per air shower and therefore improving both the triggering as well as reconstruction of low-energy showers[25] [26]

2.6 Characteristics

The performance of the SWGO design is estimated by the analysis of simulated air showers and a toy-detector design and the following assumptions are made:

1. Observatory altitude: 4700m

2. Latitude: 25° South

3. A dense array with 5000 units (shown in figure 2.2) covering an area of 88,000 m^2 with a fill-factor of 80%.

4. A sparse array with 1000 units covering an area of 221,000 m^2 with a fill-factor of 8% .

A database of gamma ray and proton induced air showers distributed in the energy range from 30 GeV to 1 PeV and evaluated at ground-level by an array of idealized detector units shown in figure 2.3 is available for study presented here.

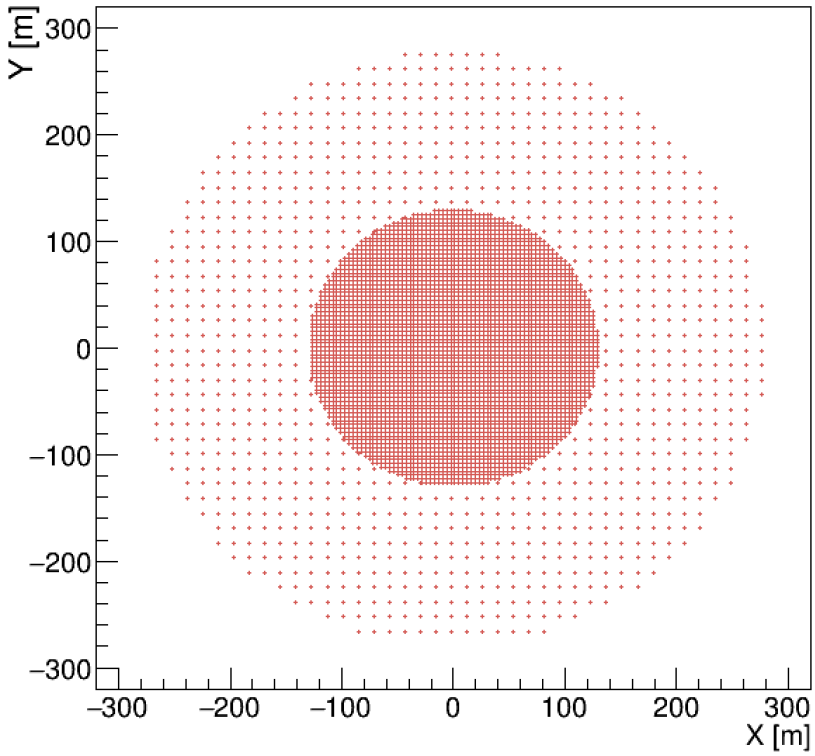

Figure 2.3: SWGO Array Configuration, [3]

Chapter 3

Gamma-Hadron Separation

A gamma ray entering the earth's atmosphere can interact with the nuclei of an atom and generate an electron-positron pair. This results in the conversion of the energy of a gamma ray into the rest masses and energies of the generated particles until the gamma ray ceases to exist. The rest mass of an electron is about 0.5 MeV/c2, that is minuscule as compared to the energy of the gamma ray, leading to the rest of the energy getting converted to kinetic energy implying that the electron and positron are both created traveling at relativistic speeds. The relativistic particles then emit more gamma rays while propagating through the atmosphere and these secondary gamma rays create more electron-positron pairs resulting in a cascade that continues until the critical energy is reached. The shower then dissipates with several thousand particles still reaching the WCDs on the ground. The photons reaching the ground

will convert to electron-positron pairs in the water. The charged particles will then emit Cherenkov radiation which triggers the PMTs inside the WCDs.

The gamma-ray induced EAS reaching the ground are overwhelmed by the "background" of cosmic-ray induced EAS which impose an experimental challenge for gamma-ray observatories to remove this background from our signal. We can discriminate air showers by observing certain characteristics specifically associated with gamma-ray showers and hadronic showers. One such characteristic is the spatial pattern of the shower observed in the detector also sometimes called the shower footprint. In gamma-ray showers, the signals at ground level are distributed rather smoothly. In contrast, hadronic showers tend to have strong signal clusters farther away from the core due to the muon travelling farther away from the shower axis, leading to a "messier" signal pattern at ground level.

3.1 Extensive Air Showers and Detector Simulation

To understand the response of the SWGO detector different sets of simulations are generated to properly model the detector for different data sets. Air shower simulation is computationally intensive and the computation time scales with the energy of the primary particle. Air showers induced by gammas and protons are simulated to the

detector level of SWGO. For the secondary particles under certain energy, a statistical sampling method is used instead of tracking each particle. This reduces computation time and makes simulation of highly energetic air showers feasible.

The showers of gammas and protons are simulated in an energy range of 30 GeV to $\sim$ 1 PeV. The particles are thrown at 0 to 65° from zenith, assuming a power law spectrum with a spectral index of -2. A model spectrum harder than typical astrophysical spectra is used to have enough statistics on high energy particles. The particles are then properly weighted to follow different spectra that are required for different analyses.

The EAS are simulated by using CORSIKA (COsmic-Ray Simulations for KAskade)[27]. The detector simulation package GEANT4 (GEometry ANd Tracking)[28] is utilized to simulate the detector response to the air shower particles for both HAWC and SWGO.

3.1.1 Gamma-Hadron Separation

It is anticipated that SWGO will achieve significant improvement in background rejection and characterization over HAWC. The shower footprints produced by gamma ray and cosmic ray have different characteristics. EAS originating from gamma rays have a significantly lower number of muons than those originating from cosmic rays.

Muons hit the WCDs further from the shower core. Thus, gamma-ray-initiated EAS are smoother, more compact, and more uniformly distributed around the shower core in comparison to the cosmic ray initiated EAS. There are several gamma-hadron variables that distinguish if the air shower particles are produced by a gamma ray or a cosmic ray. In the following, I will discuss the one I used in my study.

3.2 Parameter for Identifying Nuclear Cosmic Rays

Gamma-hadron separation is a crucial step in studying gamma-ray astronomy. The separation parameter used in this study is Parameter for Identifying Nuclear Cosmic rays (PINCness). This variable is a measure of "smoothness" of the lateral distribution function of the charge. It is defined as:

$$P = \frac{1}{N} \sum \frac{(log(q_i) - < log(q_i) >)^2}{\sigma^2_{log(q_i)}} \tag{3.1}$$

where N is total number of hits, q_i is the effective charge in the i^{th} PMT and $\sigma_{log(q_i)}$ is the uncertainty in charge. PINCness determines fluctuations within a specific annulus around the core. In gamma-ray showers, the fluctuations must be small because the lateral distribution of the charge tend to be symmetric and smoother

than in case of hadronic showers. This is evident from the distribution in Figure 3.1.

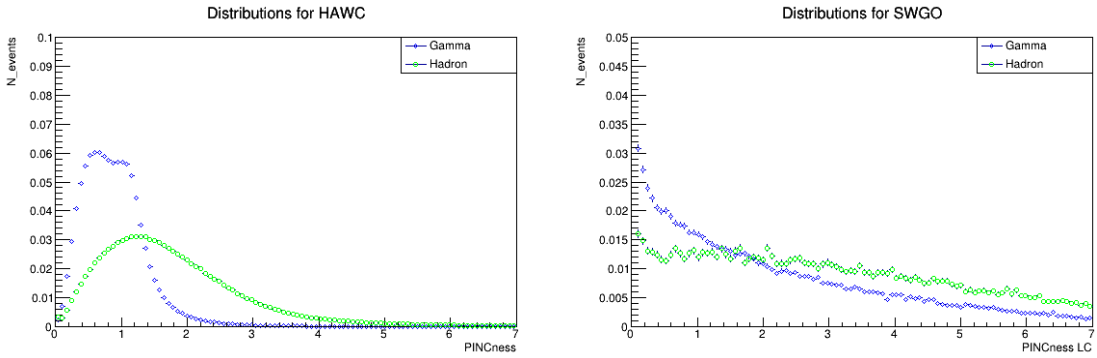

Figure 3.1: Distribution for PINCness for HAWC(left) and SWGO lower chamber (right). Blue distributions are for gamma and green for hadron. These plots are only based on on-array events, that is, true shower core falls on the array

In the SWGO detector, the bottom chamber provides a large dynamic range in the shower core, where for the highest energy gamma rays the particle density is very high. Thus, the bottom compartment can be used to provide a good estimate of the particle density. For the study presented in this report, we have only considered the signals from the PMTs in the lower chamber. Moreover, the errors $\sigma_{log(q_i)}$ here for the SWGO are assigned from a study of a simulation dataset composed of bright gamma-ray events (nHit>6000). We used a similar method as for the HAWC experiment, except the errors for HAWC were optimized from a study of the strong gamma-ray candidates from the direction of the Crab Nebula. After the SWGO begins taking data, the charge errors can also be optimized by the real gamma-like data.

Chapter 4

Analysis and Results

4.1 Energy Binning

For comparative studies with SWGO data, we have considered a binning scheme based on the true energy for on-array events where the events are thrown for a spectral index of -2.0. The simulation data is divided into 4 bins described in the table 4.1.

The simulation data sample has been grouped into 4 bins according to the logarithm of simulated true energy, as shown in figure 4.1. The distributions of Nhit with applied cuts for both HAWC and SWGO for all 4-bins are as shown in figure 4.2.

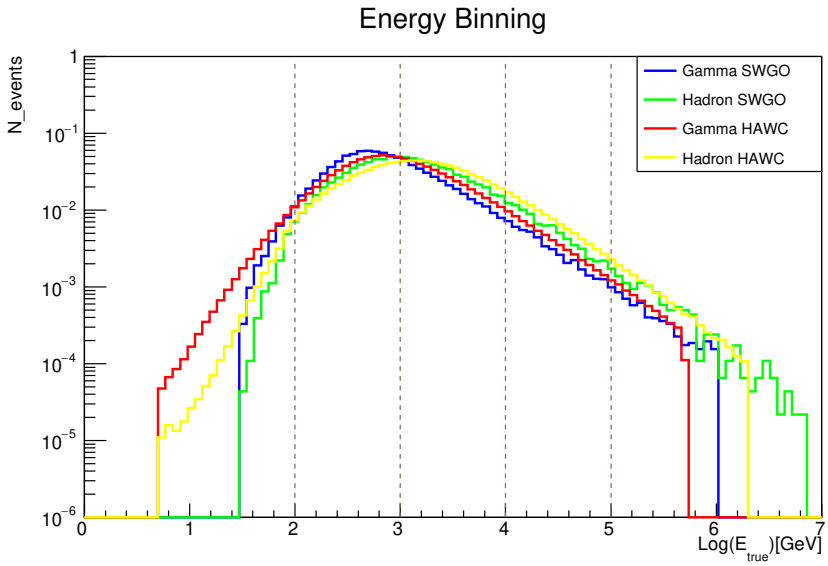

Figure 4.1: Distribution of true energy primaries triggering SWGO and HAWC. The vertical dashed lines mark the energy bin boundaries.

The figure 4.1 shows a good agreement of the spectral energy distribution of gamma-ray and proton primaries that induce air shower triggering the SWGO and HAWC array.

Bin	Energy Range
1	100 GeV- 1 TeV
2	1 TeV- 10 TeV
3	10 TeV- 100 TeV
4	$>$ 100 TeV

Table 4.1
Binning based on log of simulated true energy in GeV

The difference of the Nhit range between HAWC and SWGO is evident and expected, given the two vastly different number of PMTs and different detector configurations. The 50th, 60th, 70th, 80th and 90th percentile cuts are also shown for HAWC (black dashed-line) and SWGO (pink dashed line). The five corresponding Nhit cut values

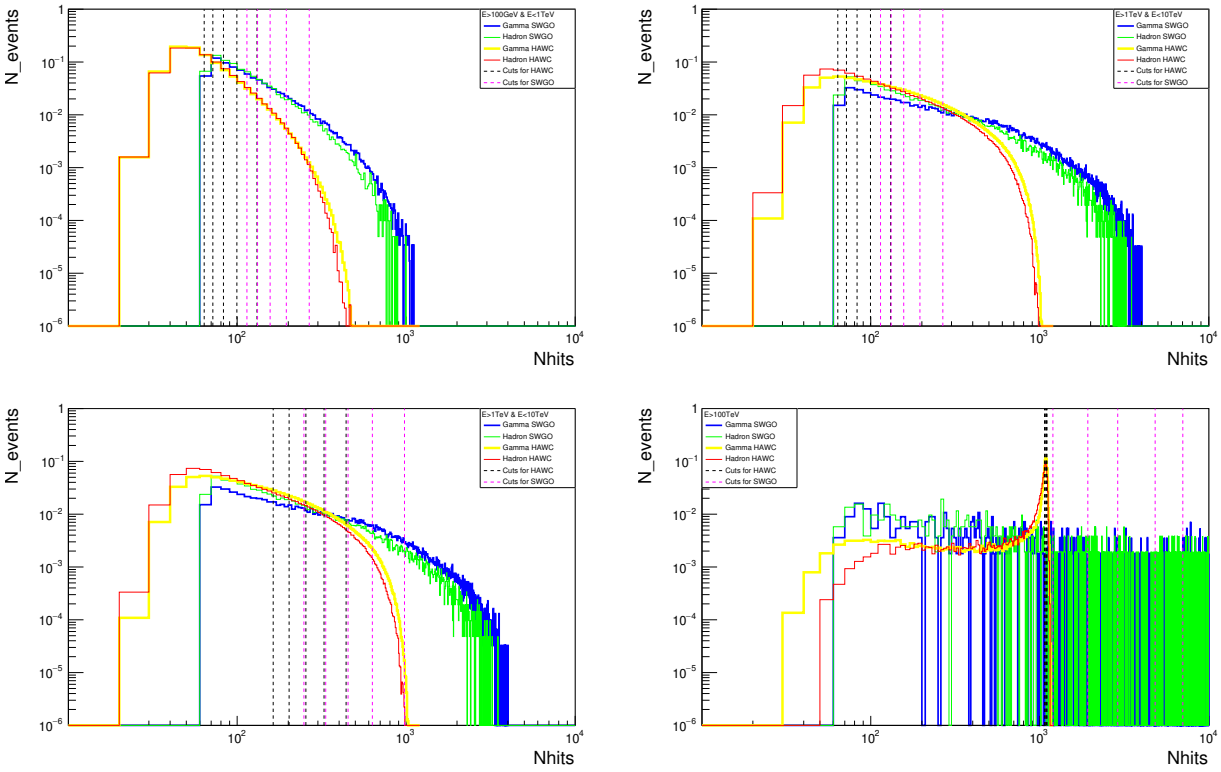

Figure 4.2: Distribution for Nhit with their corresponding cut values for percentiles $50^{th} - 90^{th}$ HAWC(black dashed-line) and SWGO(pink dashed-line).

are summarized in table 4.2 together with the number of gamma ray event surviving the cuts. The lack of statistics in the case of simulated SWGO data compared to simulated HAWC data is obvious and will make a conclusive performance comparison between the two instruments difficult if not impossible. Despite this, PINCness distributions for the five different Nhit cut scenarios are derived in each of the four true energy bands for both HAWC and SWGO. They are shown below (figure 4.3 to 4.10). The separation capability of PINCness parameter is apparent for both HAWC and SWGO with the distribution for hadronic shower footprint extending to a larger values. However an unbiased comparison of the parameter performance for HAWC

and SWGO is not possible at this time.

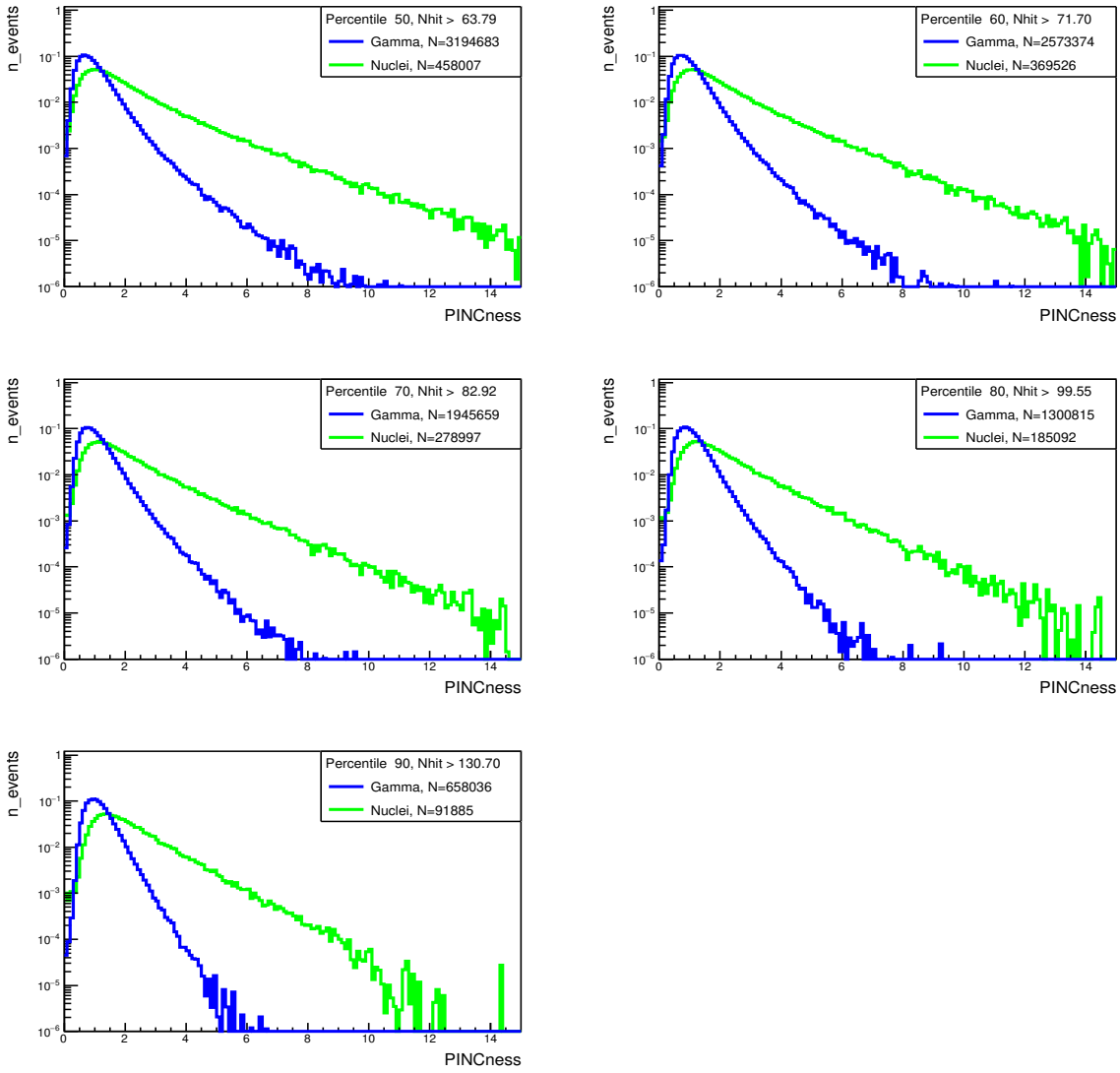

Figure 4.3: Distribution of PINCness for percentile cut on Nhit distribution for energy 100GeV-1TeV for HAWC.

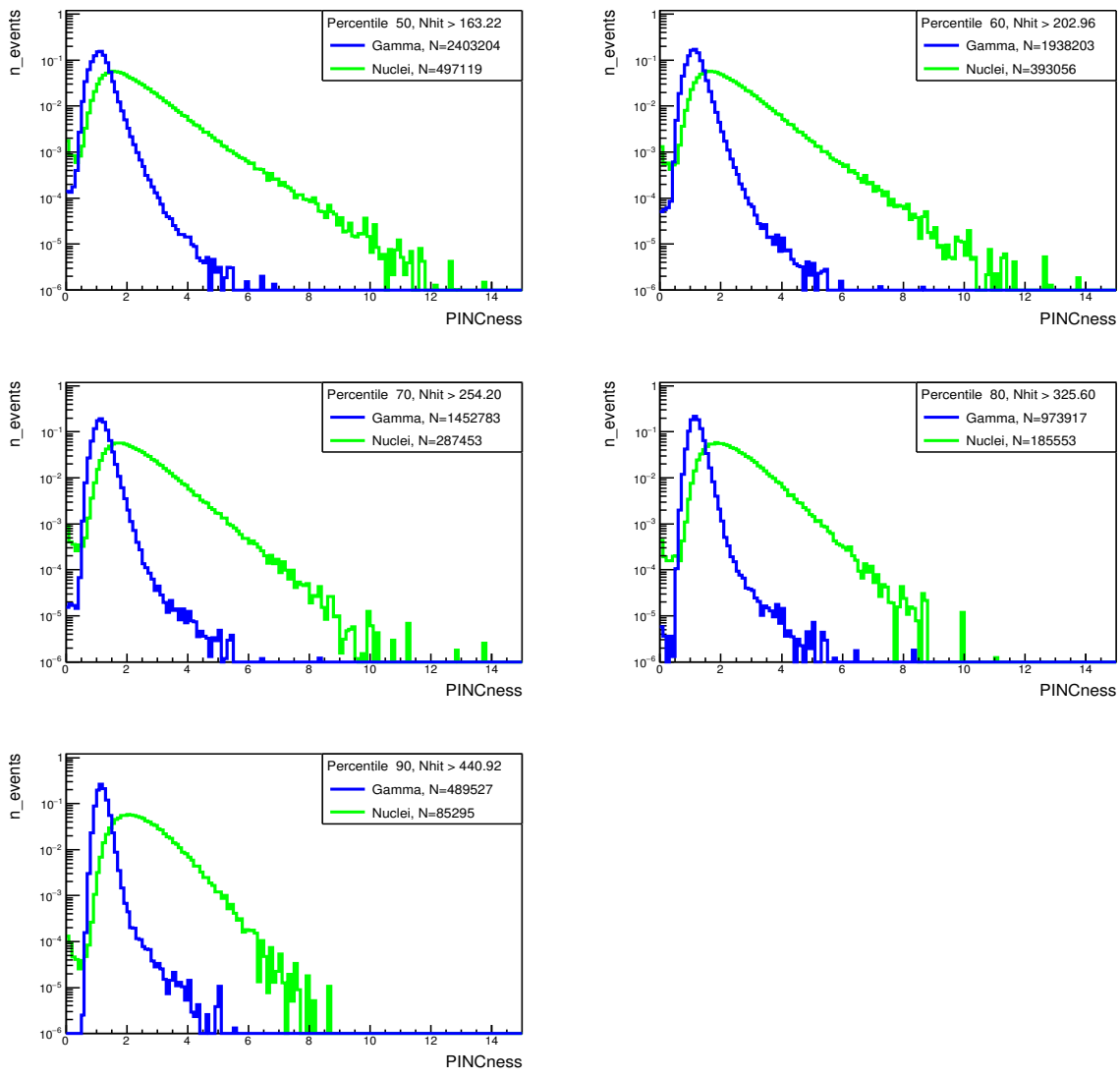

Figure 4.4: Distribution of PINCness for the $50^{th} - 90^{th}$ percentile cut on the Nhit distribution for primary particle energy 1TeV-10TeV for HAWC.

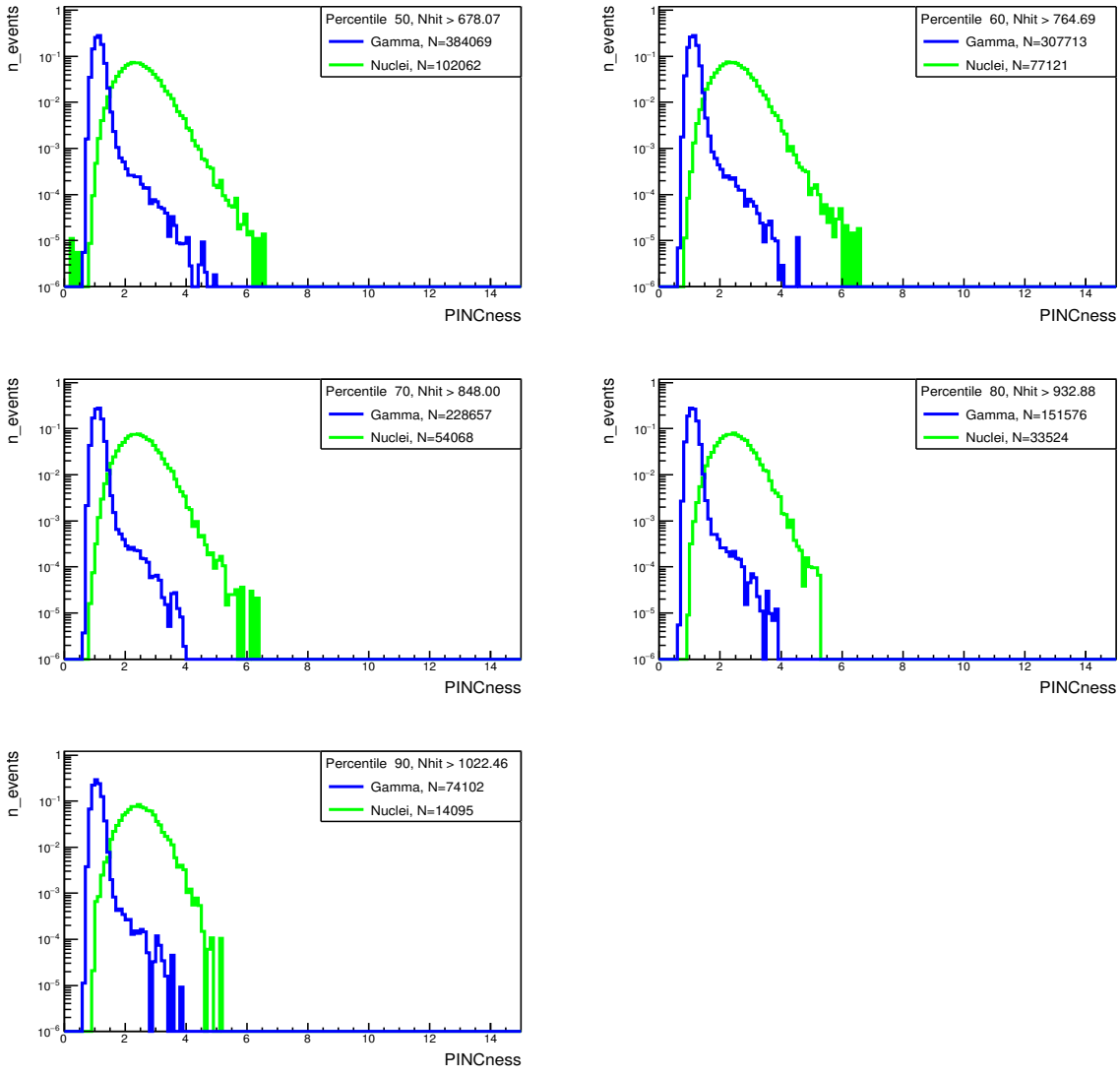

Figure 4.5: Distribution of PINCness for the $50^{th} - 90^{th}$ percentile cut on the Nhit distribution for primary particle energy 10TeV-100TeV for HAWC.

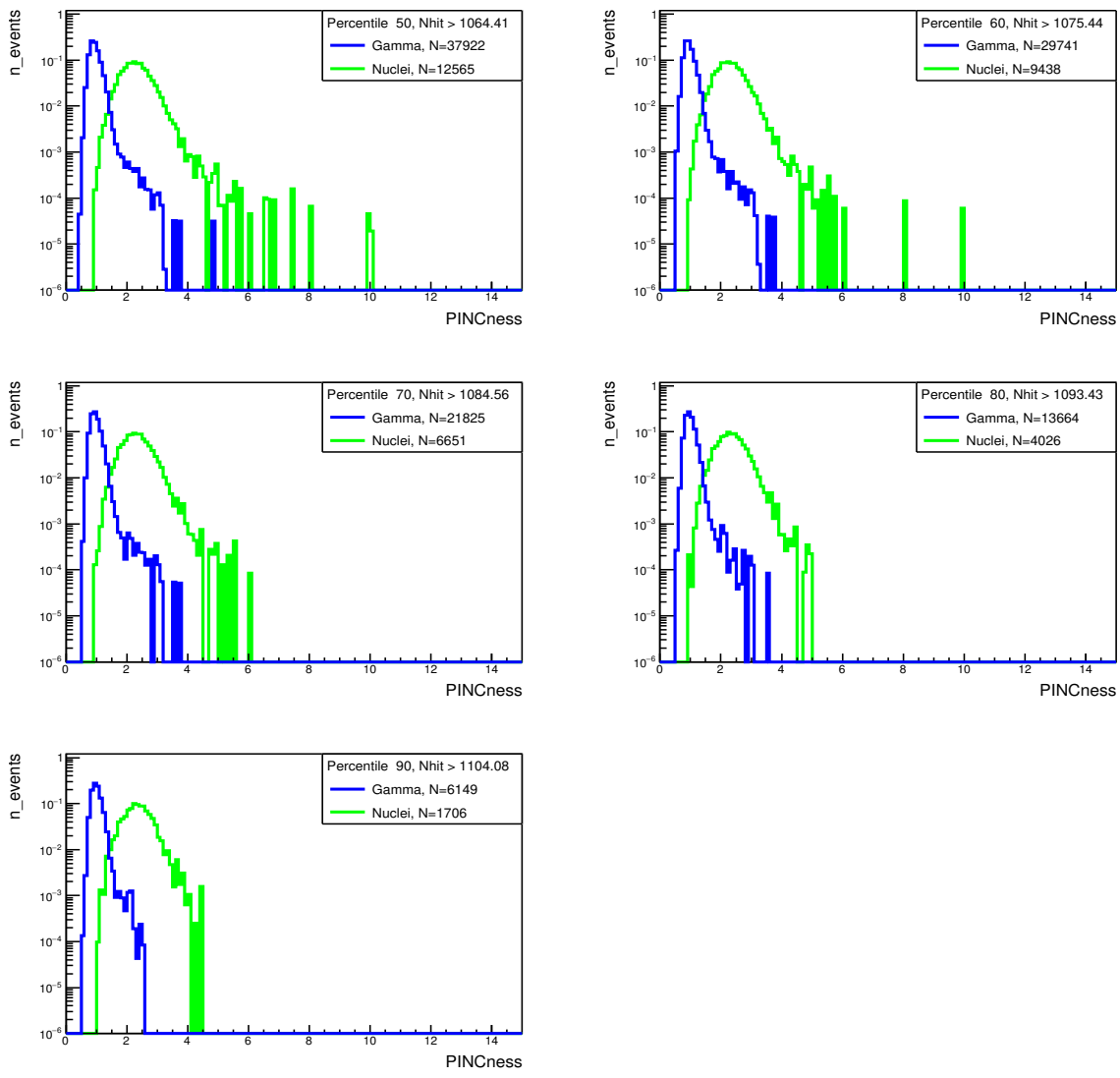

Figure 4.6: Distribution of PINCness for the $50^{th} - 90^{th}$ percentile cut on the Nhit distribution for primary particle energy $>$ 100TeV for HAWC.

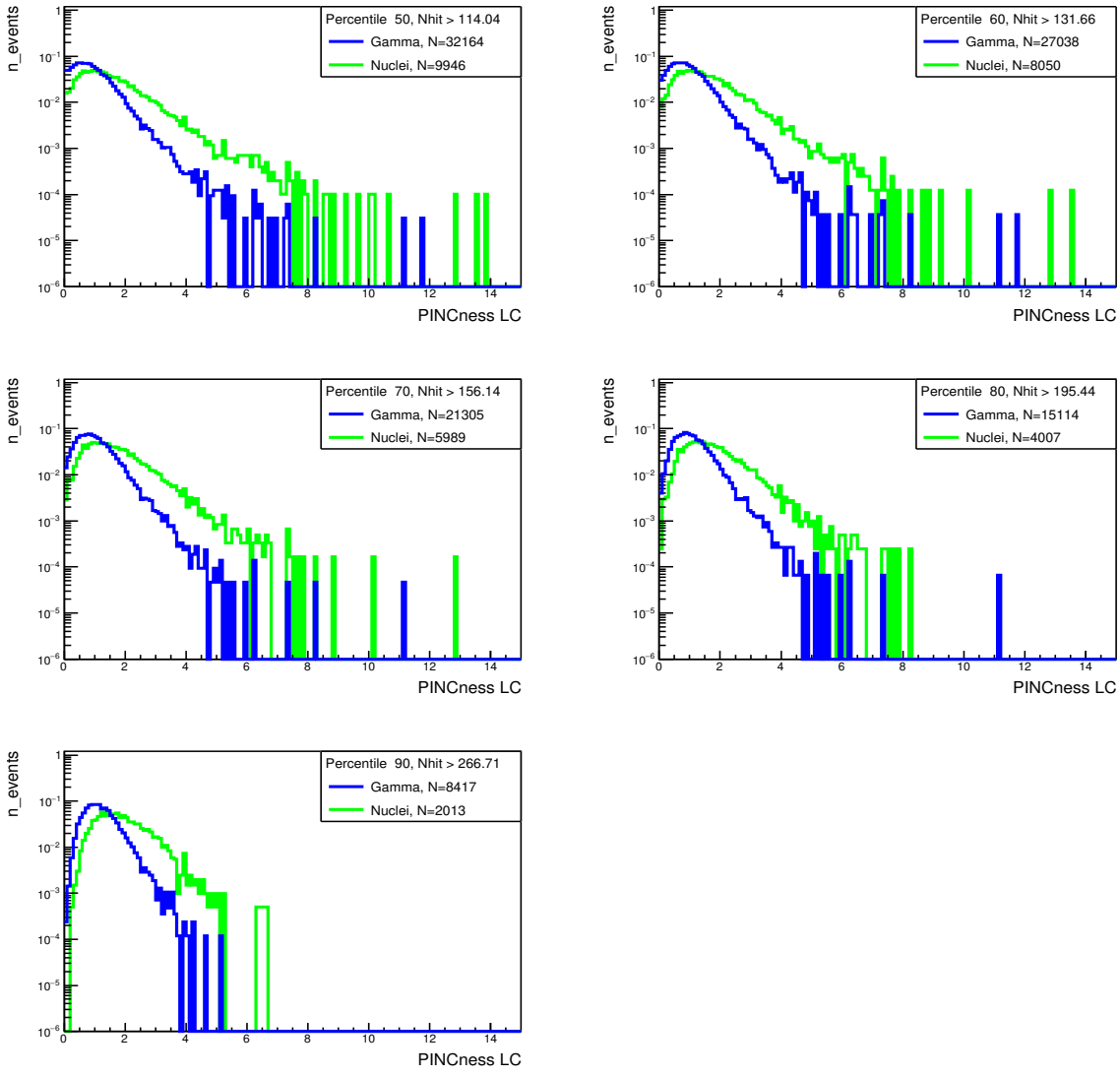

Figure 4.7: Distribution of PINCness for the $50^{th} - 90^{th}$ percentile cut on the Nhit distribution for primary particle energy 100GeV-1TeV for SWGO.

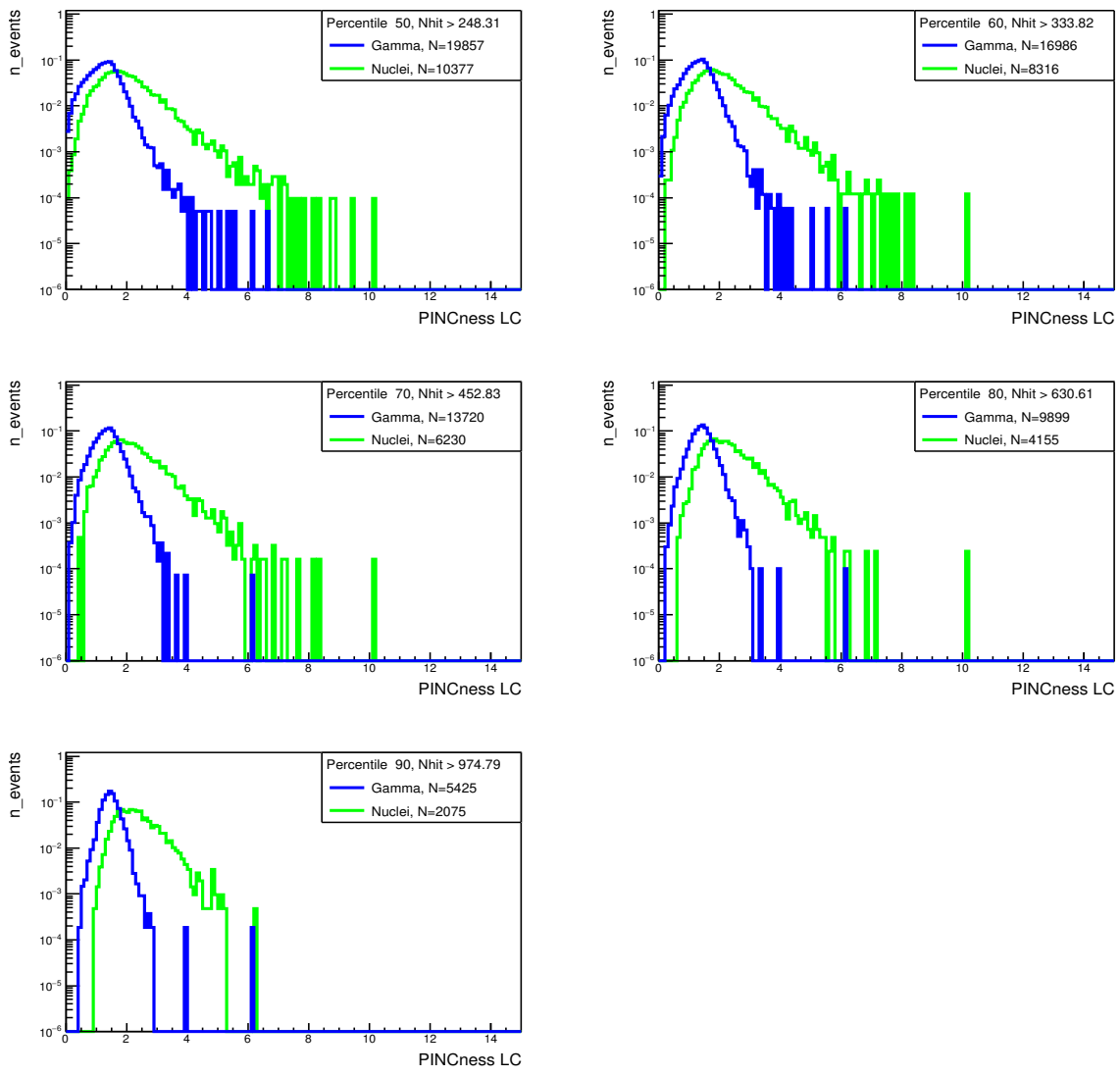

Figure 4.8: Distribution of PINCness for the $50^{th} - 90^{th}$ percentile cut on the Nhit distribution for primary particle energy 1TeV-10TeV for SWGO.

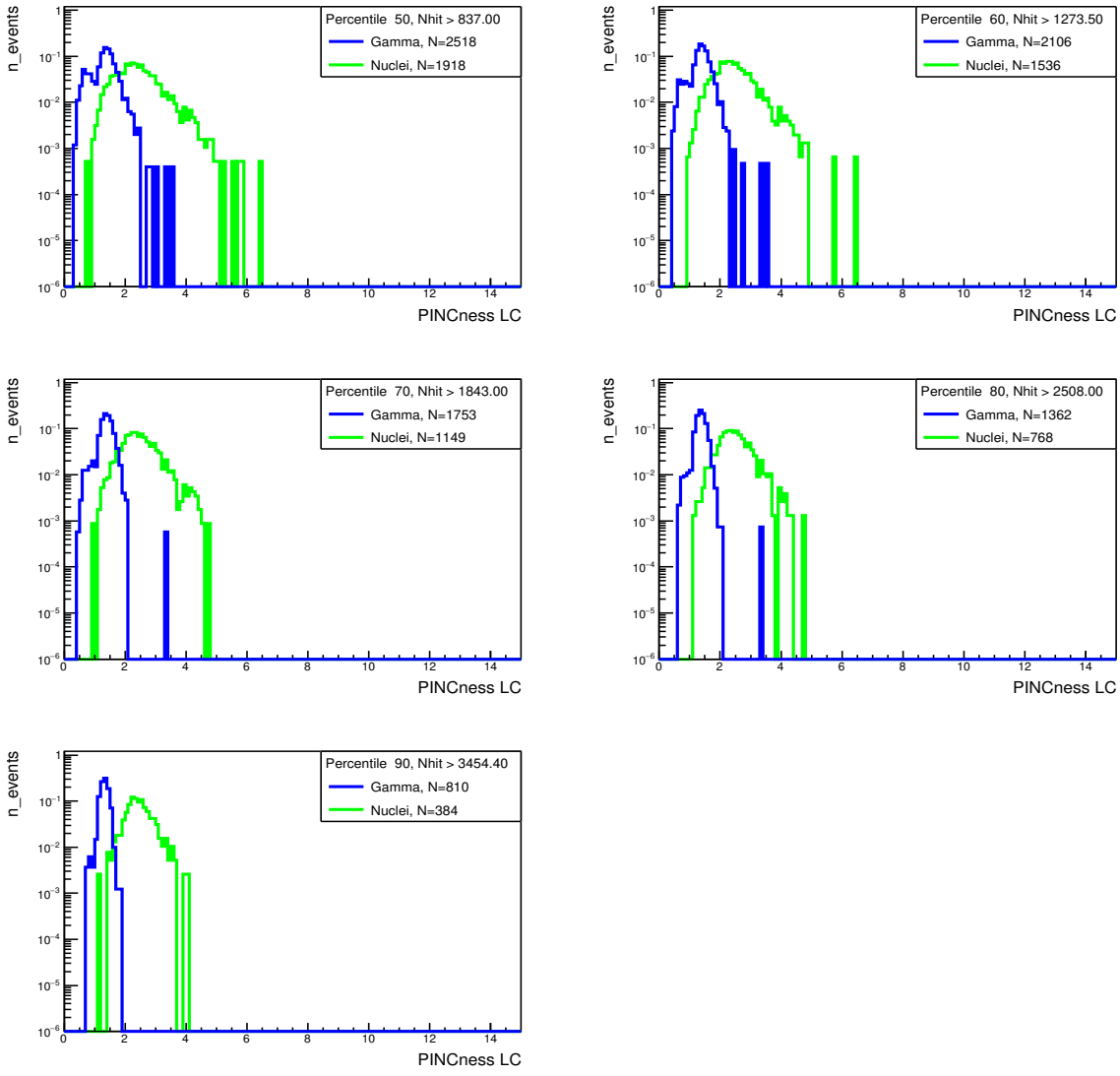

Figure 4.9: Distribution of PINCness for the $50^{th} - 90^{th}$ percentile cut on the Nhit distribution for primary particle energy 10TeV-100TeV for SWGO.

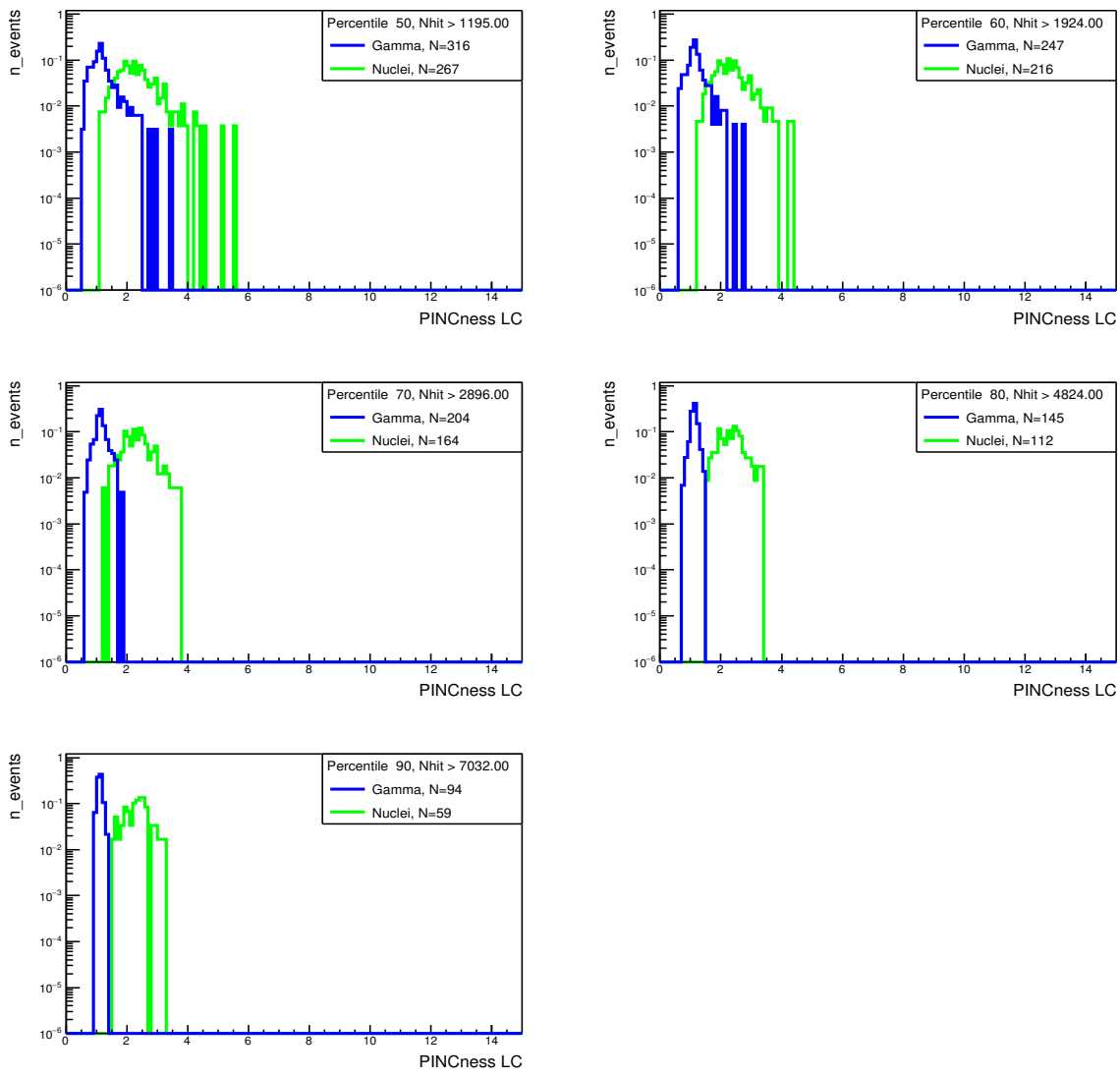

Figure 4.10: Distribution of PINCness for the $50^{th} - 90^{th}$ percentile cut on the Nhit distribution for primary particle energy $>$ 100TeV for SWGO.

Energy Bin		HAWC					SWGO				
	Percentiles	50^{th}	60^{th}	70^{th}	80^{th}	90^{th}	50^{th}	60^{th}	70^{th}	80^{th}	90^{th}
1	Nhit	63.79	71.70	82.92	99.55	130.70	114.04	131.66	156.14	195.44	266.71
	Events	3194683	2573374	1945659	1300815	658036	32164	27308	21305	15114	8417
2	Nhit	163.22	202.96	254.20	325.60	440.92	248.31	333.82	452.83	630.61	974.79
	Events	2403204	1938203	1452783	973917	489527	19857	16986	13720	9899	5425
3	Nhit	678.07	764.69	848.00	932.88	1022.46	837.00	1273.50	1843.00	2508.00	3454.40
	Events	384069	307713	228657	151576	74102	2518	2106	1753	1362	810
4	Nhit	1064.41	1075.44	1084.56	1093.43	1104.08	1195.00	1924.00	2896.00	4824.00	7032.00
	Events	37922	29741	21825	13664	6149	316	247	204	145	94

Table 4.2
Summary of Nhit cut values and corresponding number of gamma events
for different percentile for all energy bins for HAWC and SWGO.

Chapter 5

Conclusion and Outlook

This report described a study to evaluate gamma hadron separation capabilities of an early version of a possible SWGO array configuration. A gamma-hadron separation parameter optimized for HAWC that measures the smoothness of the shower footprints in the detector array (PINCness) was tested. The detectors for SWGO and HAWC are different in structure. The WCD for HAWC uses a deep single-layered design whereas the SWGO WCD tested here is a shallower double layered design. Owing to that both are expected to show different performances of the gamma-hadron separation parameter.

Simulated PINCness distributions were produced for both, the HAWC and SWGO

configurations. PINCness, despite being not optimized, still shows a reasonable distribution for SWGO. The gamma-hadron separation performance of SWGO could not be properly compared to that of HAWC however, which can be attributed to the inadequate statistics available from the limited volume of simulation data.

At first site, PINCness appears to be more easily adaptable. However, without optimization to the SWGO configuration under study, the parameter was found to underperform. A specific shortcoming that has been identified is related to the charge errors. For HAWC, they are derived based on charge fluctuation studies using events that HAWC recorded from the direction of the Crab nebula. Moreover, other ways of optimizing PINCness may be found by studying the performance of the parameter with the upper cell and/or with different annuli widths to investigate if this could improve the performance at lower gamma-ray energies we well.

Another continuation of this work is the study of other parameters. HAWC data reconstruction for example successfully uses the reduced χ^2 from fitting the Nishimura-Kamata-Greizen (NKG) function to shower footprints in the array. Because the NKG function is designed to describe purely electromagnetic showers, it tends to produce smaller χ^2 for gamma-ray induced showers. This can be utilized for gamma-hadron separation[7]. Last but not the least, the development of new gamma-hadron separation may also be possible to achieve improved gamma-hadron separation than reported here.

References

[1] https://doi.org/10.1007/978 3-030-27339-2, D. *Astroparticle Physics, 2nd edition;* Springer, 2020.

[2] https://www.mpi hd.mpg.de/hfm/CosmicRay/Showers.html. *EAS;* MPIK, 2020.

[3] Wang, X. *Private communication;* MTU, 2022.

[4] on behalf of the SWGO collaboration, H. S. *arXiv:1908.08858v1, astro-ph.HE* **2019**.

[5] *Proc. Double-layered Water Cherenkov Detector for the Southern Wide-field-of-view Gamma-ray Observatory (SWGO),, ICRC 2021*, Poster, **2021**.

[6] Schüssler, F.; the SWGO Collaboration. *astro-ph.HE* **2019**.

[7] Zhou, H. *Search for TeV Gamma-Ray Sources in the Galactic Plane with the HAWC Observatory* PhD thesis, Michigan Technological university, **2015**.

[8] Malone, K. A. *A Survey of the Highest-Energy Astrophysical Sources with the HAWC Observatory* PhD thesis, Penn State university, **2018**.

[9] Abdo, A. A. *Discovery Of Localized Tev Gamma-Ray Sources And Diffuse Tev Gamma-Ray Emission From The Galactic Plane With Milagro Using A New Background Rejection Technique* PhD thesis, Michigan State university, **2007**.

[10] `https://imagine.gsfc.nasa.gov/science/toolbox/gamma_ray_astronomy1.html`. *Gamma-ray Astronomy, NASA;* NASA, 2021.

[11] Hona, B. *Cosmic-Ray Acceleration in the Cygnus OB2 Stellar Association* PhD thesis, Michigan Technological university, **2020**.

[12] Karl-Heinz Kampert, A. A. W. *The European Physical Journal H* **2012**.

[13] Brisbois, C. A. *Understanding The Very High Energy Gamma-Ray Emission From A Fast Spinning Neutron Star Environment* PhD thesis, Michigan Techological university, **2019**.

[14] https://en.wikipedia.org/wiki/High_Energy_Stereoscopic_System. *H.E.S.S. telescope;* Wikipedia, 2022.

[15] https://en.wikipedia.org/wiki/MAGIC_(telescope). *MAGIC telescope;* Wikipedia, 2022.

[16] https://en.wikipedia.org/wiki/VERITAS. *VERITAS telescope;* Wikipedia, 2022.

[17] https://en.wikipedia.org/wiki/Cherenkov_Telescope_Array. *CTA telescope;* Wikipedia, 2021.

[18] https://en.wikipedia.org/wiki/High_Altitude_Water_Cherenkov_Experiment. *HAWC telescope;* Wikipedia, 2021.

[19] https://en.wikipedia.org/wiki/Large_High_Altitude_Air_Shower_Observatory. *LHAASO;* Wikipedia, 2021.

[20] https://en.wikipedia.org/wiki/Southern_Wide-field_Gamma ray_Observatory. *SWGO;* Wikipedia, 2021.

[21] https://www.swgo.org/SWGOWiki/doku.php?id=start. *SWGO Wiki;* Wikipedia, 2019.

[22] *Proc. Benchmarking the Science for the Southern Wide-Field Gamma-ray Observatory (SWGO)*, PoS(ICRC2021)893, **2021**.

[23] *Proc. AEROSITE: Autonomous Environmental and Scientific SWGO site Characterization Instrument*, PoS(ICRC2021)738, **2021**.

[24] *Proc. The search for high altitude sites in South America for the SWGO detector*, PoS(ICRC2021)689, **2021**.

[25] Huentemeyer, P.; the SWGO Collaboration. *Astro2020 Decadal Survey* **2020**.

[26] *Proc. Technological options for the Southern Wide-field Gamma-ray Observatory (SWGO) and current design status*, PoS(ICRC2021)714, **2021**.

[27] for Astroparticle Physics, I. *https://www.iap.kit.edu/corsika/;* Karlsruhe Institute of Technology, 2022.

[28] CERN. *https://geant4.web.cern.ch/;* CERN, 2022.

[29] Leitl, F. *Core and Energy Estimations for SWGO Using a Template-based Shower Reconstruction Method* PhD thesis, Erlangen Centre for Astroparticle Physics, **2021**.

[30] Gamma/Hadron Separation for the HAWC Observatory. Gerhardt, M. J. **2020**.

[31] *Proc. Study of water Cherenkov detector designs for the SWGO experiment*, PoS(ICRC2021)895, **2021**.

[32] *Proc. Simulating the performance of the Southern Wide-view Gamma-ray Observatory*, PoS(ICRC2021)903, **2021**.

[33] et al, R. C. *arXiv:2101.10109v2* **2021**.

[34] on behalf of the LHAASO collaboration, X. W. *https://doi.org/10.22323/1.358.0820* **2021**.

[35] Hinton, J.; Ruiz-Velasco, E. *J. Phys.: Conf. Ser. 1468 012096* **2020**.

[36] et al, D. B. *arXiv:2201.04719v1 [astro-ph.IM]* **2022**.

[37] `https://en.wikipedia.org/wiki/Gamma-ray_astronomy`. *Gamma-ray Astronomy;* Wikipedia, 2021.

[38] https://en.wikipedia.org/wiki/Propagation_of_uncertainty. *Propagation of error;* Wikipedia, 2021.